Research Article | Vol. 27, No. 4 | 18 Feb 2019 | OPTICS EXPRESS 5420
Optics EXPRESS

Wideband, high-resolution terahertz spectroscopy by light-induced frequency tuning of quantum-cascade lasers

T. Alam,[1] M. Wienold,[1,2,*] X. Lü,[3] K. Biermann,[3] L. Schrottke,[3] H. T. Grahn,[3] H.-W. Hübers[1,2]

[1] *German Aerospace Center (DLR), Institute of Optical Sensor Systems, Rutherfordstr. 2, 12489 Berlin, Germany*
[2] *Humboldt-Universität zu Berlin, Department of Physics, Newtonstr. 15, 12489 Berlin, Germany*
[3] *Paul-Drude-Institut für Festkörperelektronik, Leibniz-Institut im Forschungsverbund Berlin e. V., Hausvogteiplatz 5–7, 10117 Berlin, Germany*
[*] *martin.wienold@dlr.de*

Abstract: Near-infrared optical excitation enables wideband frequency tuning of terahertz quantum-cascade lasers. In this work, we demonstrate the feasibility of the approach for molecular laser absorption spectroscopy. We present a physical model which explains the observed frequency tuning characteristics by the optical excitation of an electron-hole plasma. Due to an improved excitation configuration as compared to previous work, we observe a single-mode continuous-wave frequency coverage of as much as 40 GHz for a laser at 3.1 THz. This represents, for the same device, a ten-fold improvement over the usually employed tuning by current. The method can be readily applied to a large class of devices.

1. Introduction

High-resolution terahertz (THz) spectroscopy is of great importance for metrology, astronomy, and atmospheric research as well as for many laboratory applications due to the vast number of molecular rotational transitions and atomic fine-structure lines in that range. The spectroscopy of such transitions relies on the availability of frequency-tunable sources with a linewidth in the MHz or sub-MHz range, a frequency coverage of ideally a few tens of GHz, and, in particular for heterodyne and non-linear spectroscopy, a sufficient level of output power. Electronic sources such as multiplied microwave oscillators typically provide a frequency coverage of about ten percent of the center frequency. However, the output power of commercially available sources drops to a few tens of microwatts when the frequency increases above 1 THz. Quantum-cascade lasers (QCLs) are therefore of particular relevance for spectroscopy above 2 THz, because they can deliver milliwatts of output power with intrinsic linewidth values in the sub-kHz range [1–4]. However, so far their frequency tuning is rather limited. The frequency tuning which can be realized by varying the driving current and/or the heat sink temperature is usually well below 10 GHz. Since many of the spectroscopic methods based on THz QCLs will immediately benefit from a larger tuning range [5–12], there is a strong motivation on developing methods which enhance the frequency tuning capability of these lasers. Several techniques have been demonstrated during recent years. Among them are external optical cavities with reported continuous tuning ranges of 12–50 GHz [13–15], micro-optomechanical cavities with 67–240 GHz [16, 17], electronic frequency tuning in multi-terminal and multi-section QCLs with 2–19 GHz [18–21], and tuning by gas condensation with 25 GHz [22] as well as by cavity pulling effects in microdisk resonators [23]. However, none of these approaches have been established so far for high-resolution spectroscopy, which may originate from the often involved complicated setups and device fabrication procedures or from non-continuous or non-reproducible frequency

#351277 https://doi.org/10.1364/OE.27.005420
Journal © 2019 Received 6 Nov 2018; revised 21 Dec 2018; accepted 4 Jan 2019; published 13 Feb 2019

Optics EXPRESS

tuning characteristics.

Near-infrared (NIR) laser excitation was exploited by several groups to manipulate the output power and frequency of mid-infrared QCLs [24–27]. Recently, a significant frequency tuning of already several GHz for continuous-wave operation was obtained for THz QCLs by unfocused NIR illumination [28,29]. Based on an improved illumination scheme for well-controlled focused excitation, we demonstrate in this work the feasibility for high-resolution molecular spectroscopy with a wide bandwidth. The following section discusses the experimental configuration and the molecular spectroscopy. In section 3, we present a physical model for the observed frequency tuning characteristics. In section 4, we compare the optical tuning effect for different devices, including a discussion of current and thermal frequency tuning, and show that a frequency coverage of up to 40 GHz is obtainable. In section 5, we eventually discuss prospects and limitations of the method.

2. Tuning setup and spectroscopic measurements

In principle, a large variety of configurations is feasible for light-induced frequency tuning (LIFT). Our experiments are based on edge-emitting QCLs, for which the laser oscillates in a ridge waveguide structure between two cleaved facets. The QCLs are uncoated Fabry-Pérot devices with optical access to both end facets. The experimental configuration is illustrated in Fig. 1(a). It consists of two parts: frequency tuning by NIR optical excitation and molecular spectroscopy with an absorption cell as well as a detector. For frequency tuning, one facet of the QCL is illuminated with focused light from a NIR diode laser. For aligning and focusing the NIR laser, we use a confocal microscope setup based on a x-y-z translation stage. For molecular

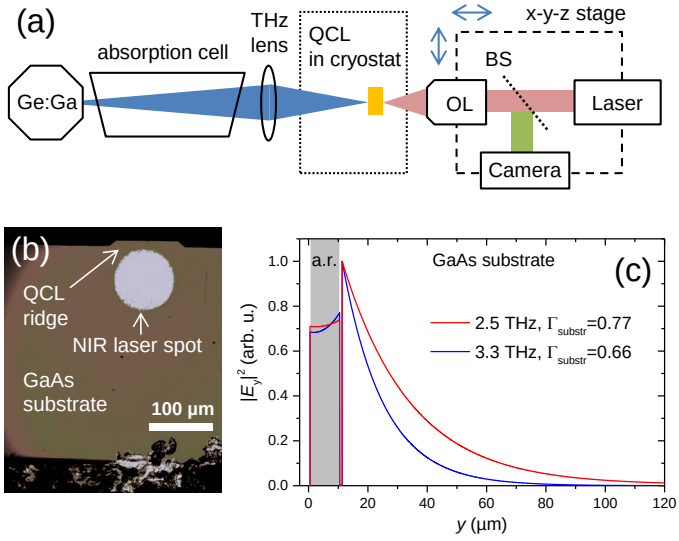

Fig. 1. (a) Schematics of the experimental setup. The QCL (yellow box) is mounted in a He-flow cryostat. BS - dichroic beamsplitter; OL - objective lens; Ge:Ga - photoconductive Ge:Ga detector. (b) Microscope image of the illuminated QCL facet. The excitation spot with a diameter of approximately 90 μm originates from a multimode diode laser emitting at 809 nm and exhibits essentially a flat-top profile. (c) Calculated profile of the waveguide mode in the vertical (epitaxial-growth) direction for different frequencies (the mode propagates perpendicular to y along the waveguide ridge). The active region (a. r.) has a height of 10 μm and corresponds to the QCL ridge structure in (b).

Optics EXPRESS

spectroscopy, the THz emission from the opposite facet of the QCL is collected by a THz lens and directed through a 60-cm-long absorption cell onto a Ge:Ga photoconductive detector.

In this work, we focus on QCLs based on single-plasmon waveguides [1, 2]. For such QCLs, the waveguide mode extends to a large part into the semi-insulating GaAs substrate. Figure 1(b) depicts a microscope image of the illuminated QCL facet showing the substrate with the ridge waveguide structure on top (which contains the active region) and the NIR laser spot. A well-defined tuning behavior is obtained by exciting the GaAs substrate in the vicinity of the ridge waveguide structure. For focused excitation of the active region, we are typically facing a strong gradual decrease of the QCL intensity as well as mode instabilities, which makes such a configuration unfavorable for spectroscopy. Figure 1(c) depicts the calculated profile of the QCL waveguide mode in the vertical (epitaxial-growth) direction for two different laser frequencies. Almost 80% of the mode intensity is guided within the GaAs substrate at 2.5 THz, while at 3.3 THz still two-thirds of the mode intensity is located in the substrate. Hence, it is rather intuitive that manipulating the optical properties of that region will change the behavior of the QCL.

For LIFT measurements, the QCLs are operated at constant driving current and temperature. The diode laser current is ramped from below threshold to the final level, and the signal of the Ge:Ga detector is recorded with a fast data acquisition device (CDAQ, National Instruments). Depending on the sweep rate, the acquisition of a single spectrum takes typically 20–100 ms. The maximum illumination intensity for frequency tuning is then determined either by the complete quenching of the QCL emission, an illumination-induced mode transition, or the power limitations of the diode laser. We obtained the largest tuning effects with a multi-mode diode laser emitting up to several Watts of optical power at 809 nm (DILAS, I2F2S22-808-SS14.2).

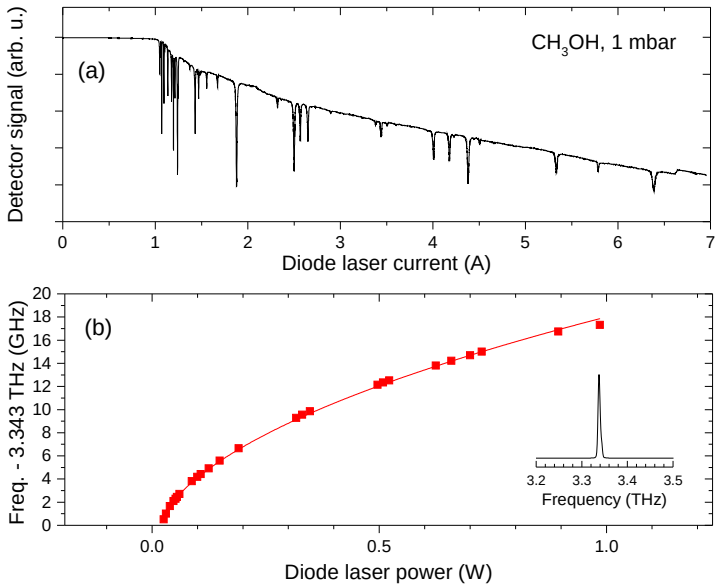

Fig. 2. (a) Detector signal as a function of the diode laser current for 1 mbar of methanol. The QCL is operated at a constant current of 380 mA at 37 K (threshold value: 300 mA). (b) QCL frequency as a function of the incident diode laser power. Square dots refer to the frequencies of the methanol absorption lines in (a), which were identified according to the JPL molecular catalogue. Solid line: square-root parameter fit to the data according to Eq. (1). Inset: QCL emission spectrum (without NIR excitation) as measured with a Fourier transform spectrometer (3 GHz resolution) confirming single-mode operation.

Optics EXPRESS

The emission of this laser is focused with the help of a 30-mm lens and a ten-fold objective into a 90-μm spot on the QCL facet. Note that the average optically power remains typically well below 0.5 W during the measurements, which compares to an electrical power dissipation of 1–3 W of the QCLs. With respect to cryogenic cooling, optical heating is therefore mostly negligible. Due to local heating of the active region during the sweep, the optimal spot position is typically found somewhat lower than indicated in Fig. 1(b) for large excitation levels.

The results of a spectroscopic measurement with a QCL operating at 3.3 THz are shown in Figs. 2(a) and 2(b). The particular device has been chosen here due to the absence of atmospheric absorption features in that frequency range. Therefore, the behavior of the QCL under optical excitation is very clearly revealed. The short cavity length of 1 mm facilitates single-mode operation of the QCL [cf. inset of Fig. 2(b)], which is a precondition for this kind of spectroscopy. In Fig. 2(a), the detector signal is displayed as a function of the driving current of the NIR diode laser. Tuning sets in above threshold of the diode laser at 1 A, and a large number of methanol absorption lines is observed in the detector signal together with a gradual decrease of the QCL output intensity. The maximum tuning range is restricted by a mode hop for that QCL at a diode laser current of 6.5 A. For a well-known species such as methanol, the individual lines of the spectral fingerprint can be identified according to a molecular catalog. With such a frequency calibration, the tuning behavior can be precisely determined as shown in Fig. 2(b). We found that the QCL frequency ν as a function of the driving current I of the diode laser is in most cases very well approximated by a square root dependence above threshold. Since the power P of the diode laser scales approximately linearly with current above threshold, the frequency increases as

$$\nu(P) = \nu_0 + a_L\sqrt{P} \tag{1}$$

The parameter ν_0 represents the unperturbed QCL frequency and a_L the LIFT proportionality constant, which will be derived later.

Figure 3 depicts a frequency-calibrated transmission spectrum, for which the data of Fig. 2 were divided by a reference spectrum for an empty gas cell. For comparison, the simulated transmission spectrum based on the molecular catalog of the Jet Propulsion Laboratory (JPL) is shown [30], which underlines the spectroscopic quality of the experimental data obtained with LIFT. Further experimental results regarding different devices as well as a discussion of thermal

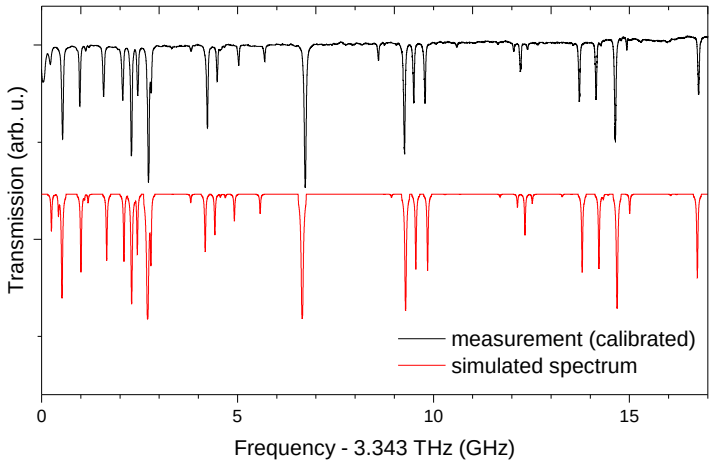

Fig. 3. Measured transmission spectrum after frequency calibration (top) and simulated methanol spectrum (bottom).

Optics EXPRESS

and current tuning parameters are presented in section 4.

3. Physical model for light-induced frequency tuning

In this section, we present a physical model for the frequency tuning mechanism for optical excitation of the substrate. Therefore, we consider a one-dimensional Fabry-Pérot cavity consisting of GaAs. By illuminating a semiconductor with light above the band gap, electron-hole pairs are generated. Immediately after generation, these pairs form a plasma state of unbound electrons and holes, which subsequently decays via various channels. Since the operating temperatures are below 100 K, we will neglect carrier diffusion. We further neglect surface and Auger recombination, and assume that the electron density n_e equals the hole density n_h. In the steady state, the plasma density $n_{\mathrm{eh}} = n_e = n_h$ is then described by [31]

$$\frac{n_{\mathrm{eh}}}{\tau_{\mathrm{nr}}} + B n_{\mathrm{eh}}^2 = G \,, \tag{2}$$

where G, τ_{nr}, and B denote the generation rate, the non-radiative lifetime and the bimolecular recombination parameter, respectively. At low temperatures, non-radiative recombination is strongly reduced [32], while bimolecular recombination becomes enhanced [33]. The concentration of the electron-hole plasma becomes approximately

$$n_{\mathrm{eh}} = \sqrt{\frac{G}{B}} \,. \tag{3}$$

Due to absorption, G decreases exponentially in the semiconductor with

$$G(z) = G_0 \exp(-\alpha z) \,. \tag{4}$$

Here, G_0 denotes the generation rate at the surface, α the absorption coefficient at the particular excitation wavelength, and z the distance from the facet along the waveguide. Reabsorption of the undirected luminescence, which might cause a small reduction of the effective absorption coefficient, is neglected for the sake of simplicity. The generation rate per unit volume is related to the incident photon flux S_0 (number of photons per time and area) by $G_0 = \alpha S_0$. The presence of the electron-hole plasma changes the refractive index of the semiconductor. The local dielectric constant is given by

$$\varepsilon(z) = \varepsilon_s \left(1 - \frac{\omega_p^2}{\omega^2}\right) \,, \tag{5}$$

where $\varepsilon_s = n_s^2$ denotes the dielectric constant of the GaAs substrate without excitation, $\omega = 2\pi\nu$ the angular frequency of the QCL, and ω_p the plasma frequency given by

$$\omega_p^2 = \frac{n_{\mathrm{eh}}(z) e^2}{\varepsilon_0 \varepsilon_s m^*} \,. \tag{6}$$

Here, e denotes the electron charge, ε_0 the vacuum permittivity, and m^* the effective electron mass. For the sake of clarity, we assume in the following that ε_s and n_s are real-valued.

Figure 4(a) illustrates the behavior of the dielectric constant in the substrate close to the facet for different photon fluxes. For small fluxes, only the real part of the refractive index in the vicinity of the facet ($z = 0$) is affected. Above a certain photon flux, a transition from a dielectric to a metallic behavior takes place at the position where the plasma frequency ω_p equals the QCL frequency. With increasing photon flux, this transition moves deeper into the cavity. The resulting shift of the cavity resonance can be numerically calculated with the transfer matrix method [34]. This is possible without further approximations by virtually dividing the excited

Optics EXPRESS

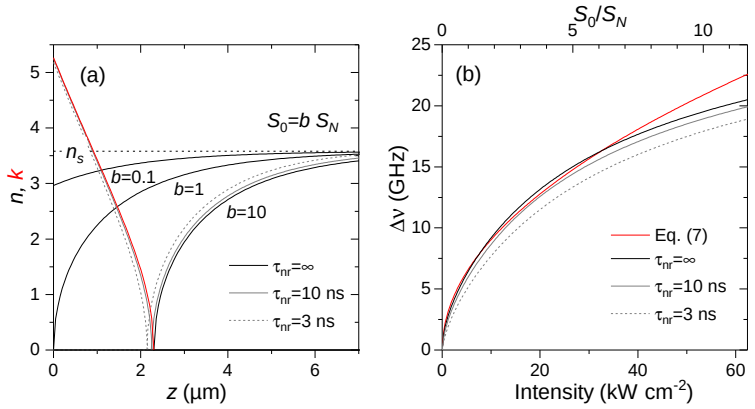

Fig. 4. (a) Calculated change of the real part of the refractive index close to the facet of the excited GaAs substrate for normalized incident photon fluxes $S_0 = bS_N$, where S_N is the photon flux for which $\varepsilon = 0$ at the surface ($z = 0$). For $b = 10$, the calculated change of the imaginary part of the refractive index is also shown, as well as further results for different values of τ_{nr}. (b) Calculated shift of the resonance frequency as a function of intensity ($\hbar\omega_{\mathrm{NIR}} S_0$) for a one-dimensional cavity. Numerical results are depicted for different values of τ_{nr}. The excitation wavelength is 810 nm, $L = 1$ mm, $\nu = 3.3$ THz, $\alpha = 10^4$ cm^{-1}, $\varepsilon_s = 12.8$, and $B = 1.8 \times 10^{-8}$ cm^3 s^{-1} [35].

region into a large number of stratified layers. The outcome of such a simulation is illustrated in Fig. 4(b). Providing that the excitation volume is small compared to the THz wavelength, it is also possible to derive an approximate, analytic expression within the transfer matrix formalism (see Appendix). Eventually, the outcome is a rather simple expression for the frequency shift $\Delta\nu$

$$\Delta\nu \approx \frac{e^2}{2\pi^2\varepsilon_0\varepsilon_s m^*}\frac{1}{L\nu}\sqrt{\frac{S_0}{B\alpha}}\,, \tag{7}$$

where we neglected non-radiative recombination. Here, ν denotes the unperturbed QCL frequency and L the physical cavity length. The frequency shift according to Eq. (7) is illustrated in Fig. 4(b) as a red line. It resembles the experimentally observed square root dependence and is in reasonable agreement with the corresponding exact numerical simulations even for rather large excitation intensities. Therefore, Eq. (7) can be used as a general estimate for the tuning range of a LIFT configuration. The same figure depicts the numerical results for different values of τ_{nr}. Since non-radiative recombination causes a linear component in the tuning characteristics which is experimentally not observed, we conclude that the non-radiative contribution is small in our configuration (with $\tau_{\mathrm{nr}} \gtrsim 3$ ns, where the particular value of τ_{nr} might vary for different GaAs substrates). If we rewrite Eq. (7) in terms of the excitation power $P = \hbar\omega_{\mathrm{NIR}} S_0 A$, we obtain

$$\Delta\nu \approx \frac{e^2}{2\pi^2\varepsilon_0\varepsilon_s m^* L\nu\sqrt{\hbar\omega_{\mathrm{NIR}} AB\alpha}}\sqrt{P} = a_L\sqrt{P}\,. \tag{8}$$

Here, $\hbar\omega_{\mathrm{NIR}}$ represents the photon energy and A the excitation area.

We explain the experimentally observed gradual decrease of the QCL output power for larger NIR illumination powers by a local heating of the active region, which results in a reduction of the gain, and a decrease of the cavity Q factor, which in turns increases the threshold gain. In contrast to the shift of the main cavity resonance, the decline of the Q factor cannot be easily recovered in a one-dimensional treatment.

Optics EXPRESS

Another aspect which becomes relevant for large tuning ranges is the relative stability of the NIR laser power. According to Eq. (8), power fluctuations δP will result in frequency fluctuations $\delta\nu$ of

$$\delta\nu = \frac{\Delta\nu}{2}\frac{\delta P}{P} \,. \tag{9}$$

Achieving 5 MHz resolution over a 50 GHz tuning range requires hence a relative power stability of 2×10^{-4} within the acquisition bandwidth, while the same resolution for a 5 GHz tuning range can be obtained already for a ten times worse stability level.

Since the tuning is caused by the optical generation of an electron-hole plasma, the LIFT method is intrinsically fast. Bimolecular recombination times for relevant excitation densities ($n_{\mathrm{eh}} > 10^{16}$ cm^{-3}) are in the nanosecond to sub-nanosecond range.

4. Comparison of light-induced, current and thermal frequency tuning effects

We successfully performed experiments with QCLs emitting at 2.5, 3.1, and 3.3 THz (referred to devices A–C in the following). The devices are Fabry-Pérot lasers with single-plasmon waveguides. For each QCL, we could identify one or two single-mode operation regimes at operating temperatures between 40 and 60 K. The frequency can be tuned within 1–4 GHz by changing the QCL driving current, where the smallest and largest tuning ranges are obtained for the 2.5 and 3.1-THz device, respectively. An overview of the current and temperature tuning parameters is given in Table 1. Note that a temperature increase leads to a negative frequency shift, while optical excitation and an increase of the QCL current lead to a positive frequency shift. Therefore, we rule out that LIFT is caused by a temperature effect. A frequency shift due to the optically induced heating of the QCL might play a compensating role. However, this effect has to be minor, since even the maximum thermal frequency shift over the whole operating temperature range of the QCLs is still about one order of magnitude smaller than the optically induced frequency shift.

The largest optical tuning range was observed for a 660-μm-long QCL emitting at 3.1 THz (device B), which was illuminated with up to 3.3 W (approximately 50 kW cm^{-2}). The QCL exhibits single-mode operation in one of two modes at 3.10 THz and 3.15 THz , with LIFT tuning ranges of about 34 and 40 GHz, respectively. Figure 5(a) depicts the methanol transmission spectrum for the high-frequency mode of this device. The LIFT range of almost 40 GHz was technically limited by the available power of the diode laser. In order to resolve all the lines, the spectrum is displayed versus the square root of the optical power.

Figure 5(b) depicts the frequency shift as a function of the normalized power for all three devices for the modes with the largest LIFT range, where the various absorption lines have been

Table 1. Current and temperature tuning parameters for the investigated QCLs: maximum frequency coverage $\Delta\nu_{I_{\mathrm{QCL}}}$ for a variation of the QCL current (I_{QCL}) and $\Delta\nu_T$ for a variation of the temperature (T); tuning coefficient $d\nu/dI_{\mathrm{QCL}}$ for frequency and $d\nu/dI_{\mathrm{QCL}}$ for temperature. The last column contains the maximum LIFT range $\Delta\nu_{\mathrm{LIFT}}$. The active region design of the corresponding QCLs are given in the respective references. Devices B and C are fabricated from different wafers with small variations of the layer thicknesses.

QCL	ν (THz)	$\Delta\nu_{I_{\mathrm{QCL}}}$ (GHz)	$d\nu/dI_{\mathrm{QCL}}$ (GHz/A)	$\Delta\nu_T$ (GHz)	$d\nu/dT$ (MHz/K)	$\Delta\nu_{\mathrm{LIFT}}$ (GHz)
A [36]	2.5	1.3	+30	1.8	−103	9.7
B [37]	3.1	3.8	+39	5.0	−238	39.4
C [37]	3.3	2.3	+19	3.5	−172	16.8

Optics EXPRESS

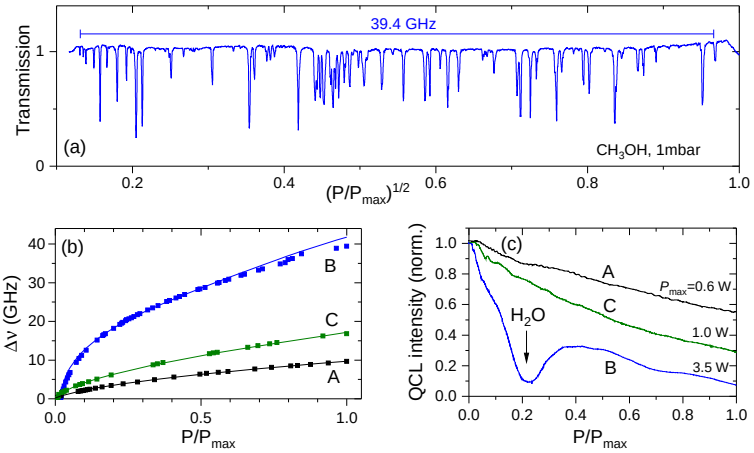

Fig. 5. (a) Methanol transmission spectrum as obtained with a 0.66-mm-long 3.1-THz QCL (device B) operated at 40 K and 295 mA. The transmission is displayed versus the square root of the normalized NIR power. (b) Frequency calibration for the modes with the largest LIFT range of each laser according to the JPL molecular catalog revealing a spectral coverage of almost 40 GHz for device B. The solid lines refer to fits to Eq. (1). (c) Normalized QCL intensity as a function of the normalized NIR power. The labeled dip in the characteristics of device B is due to atmospheric water absorption.

assigned according to the JPL molecular catalog. For devices A and C, the tuning behavior follows almost perfectly a square root dependence, while for device B certain deviations are observed as expected for very large tuning ranges [cf. Fig. 4(b)]. Figure 5(c) depicts the decrease of the QCL intensity with increasing excitation power. As discussed previously, the reason for this behavior might be an increase of the threshold gain due to the local heating of the device or a reduction of the quality factor of the QCL cavity due to the selective excitation of the substrate or the inhomogeneity of the plama excitation.

Table 2 summarizes the results obtained for the three devices. With the exception of the shortest device B, the maximum tuning range was determined by longitudinal-mode transitions of the QCLs. We found that the tuning behavior is rather well predicted by the one-dimensional model. Despite small variations of the tuning coefficient a_L for the different modes of each QCL,

Table 2. Single-mode frequency coverage by LIFT for the three QCLs.

QCL	L (mm)	$\nu_{\min} - \nu_{\max}$ (THz)	$\Delta\nu_{\mathrm{LIFT}}$ (GHz)	$P_{\max}$ (W)	a_L (GHz W$^{-1/2}$)
A	1.52	2.498–2.506	8.7	0.6	16.8
		2.523–2.533	9.7	0.6	15.1
B	0.66	3.091–3.125	33.9	2.2	24.6
		3.147–3.186	39.4	3.3	23.5
C	1.00	3.344–3.360	16.8	1.0	19.3
		3.382–3.396	14.2	0.9	16.7

Optics EXPRESS

the experimental observations agree with the predicted frequency and inverse-length dependence as well as the already discussed square root power dependence. For comparison, the theoretical values for a_L which correspond to frequency and length of lasers A, B, and C according to Eq. (8) are 9.5, 18.2, and 10.9 GHz $W^{-1/2}$, respectively (with parameters as in Fig. 4).

5. Future prospects

Since single-mode operation is facilitated for shorter cavities in combination with a stronger LIFT effect [cf. Eq. (7)], a further decrease of the cavity length may enhance the tuning range significantly. While we already obtained a combined bandwidth of 72 GHz for the 3.1-THz QCL, a future milestone will be a LIFT range which exceeds the longitudinal mode spacing. Then, the total continuous frequency coverage will be given by the mode spacing times the number of modes for which single-mode operation is achievable. Note that the gain bandwidth of the active-region structure can easily cover several hundred GHz to more than 1 THz for particular broadband designs [38]. We expect that additional noise-reducing measures will become necessary for molecular spectroscopy with a LIFT bandwidth significantly larger than 40 GHz in order to mitigate the relative power noise of the NIR laser and to maintain the frequency fluctuations according to Eq. (9) sufficiently small.

While the presented results are all based on the configuration shown in Fig. 1 (a), there is indeed a high flexibility in implementing the basic principle. By direct coupling to an optical fiber, compact and robust setups without a microscope are feasible [29]. If a smaller maximum tuning range is acceptable, a single-mode diode laser can serve as an alternative to a high-power, multimode diode laser. Such diode lasers can be focused into a diffraction-limited spot, providing large power densities. Using a single-mode diode laser at 807 nm, we were able to obtain a tuning of already 15 GHz for device B with an incident power of only 200 mW.

Note that direct excitation of the active region results in most cases in instable operation and cannot be easily exploited for spectroscopy. Therefore, some limitations of the method toward higher frequencies are expected. As illustrated in Fig. 1(c), the waveguide mode becomes stronger confined to the active region with increasing frequency. While almost 80% of the optical mode are found in the substrate for QCLs at 2.5 THz, this number decreases to values below 50% above 5 THz. If the mode is then confined mainly in the active region, the optical excitation of the substrate below the ridge waveguide structure will only cause a small perturbation of the main cavity resonance. Hence, large-range optical tuning by substrate excitation might become impossible above a certain frequency.

6. Summary

We demonstrated that spatially well-controlled optical excitation of THz QCLs enables wideband high-resolution spectroscopy, where the spectral coverage exceeds the frequency range for current and temperature tuning by about one order of magnitude. The method is intrinsically fast, since it relies not on a thermal effect, but on the optical excitation of an electron-hole plasma in the QCL substrate. In combination with a fast detector, high-resolution molecular spectra covering several tens of GHz are obtained on a millisecond time scale. The method provides a large flexibility in its implementation and can be readily applied to a large class of devices.

Appendix: derivation of the tuning equation

We consider a resonator of length L with sections A and B, where B is the section which is optically excited (cf. Fig. 6). We aim at deriving an analytic approximation for the shift of the transmission maxima, which will eventually yield the tuning equation [Eq. (7)]. Since the plasma excitation takes place on a length scale much smaller than the wavelength of the QCL and since the change of the dielectric constant can be very large, the problem cannot be covered in the

Optics EXPRESS

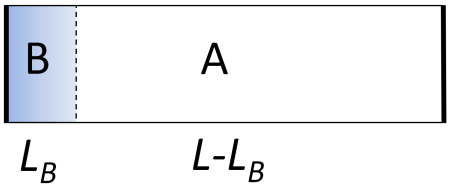

Fig. 6. Schematics of the considered two-section resonator. Section B is optically excited while A remains unaffected. The thick black lines mark the rear and front facet of the cavity.

framework of a scalar Eikonal equation. The following derivation starts with the rather general transfer-matrix formalism for stratified media, as it is routinely used to calculate for instance the transmission and reflection spectra of layered structures [34]. Within this framework, the relation of the electric and magnetic field strengths E_1 and H_1 on the left-hand side of the resonator with E_0 and H_0 on the right-hand side is given by two coupled equations, which are linear with respect to the field components. For a single dielectric layer under normal incidence, the matrix notation of these equations reads

$$\begin{pmatrix} E_1 \\ H_1 \end{pmatrix} = \begin{pmatrix} \cos(k_l l) & iZ_l \sin(k_l l) \\ \frac{i}{Z_l} \sin(k_l l) & \cos(k_l l) \end{pmatrix} \begin{pmatrix} E_0 \\ H_0 \end{pmatrix} . \tag{10}$$

Here, $Z_l = \sqrt{\mu_0/\varepsilon_l \varepsilon_0}$ denotes the wave impedance of the layer, l the thickness, and $k_l = n_l k_0$ the wavevector. In order to avoid imaginary matrix elements, we perform a base transformation $(E_i, H_i) \rightarrow (\tilde{E}_i, \tilde{H}_i)$ with $\tilde{E}_i = -i\frac{\sqrt{\varepsilon_0}}{\sqrt{\mu_0} k_0} E_i$ and $\tilde{H}_i = H_i$. The transfer matrix becomes then

$$M_l = \begin{pmatrix} \cos(k_l l) & \frac{1}{k_l} \sin(k_l l) \\ -k_l \sin(k_l l) & \cos(k_l l) \end{pmatrix} . \tag{11}$$

The transfer matrix M of the composed cavity is obtained as the product of the transfer matrices $\mathcal{A}$ and $\mathcal{B}$ referring to sections A and B

$$M = \mathcal{B} \cdot \mathcal{A} = \begin{pmatrix} M_{11} & M_{12} \\ M_{21} & M_{22} \end{pmatrix} . \tag{12}$$

The transmission coefficient for the cavity is given by

$$t = 2ik_0 e^{-ik_0 L} \frac{1}{-M_{21} + k_0^2 M_{12} + ik_0 (M_{11} + M_{22})} . \tag{13}$$

We first have to find the transfer matrices $\mathcal{A}$ and $\mathcal{B}$ in order to determine M. Subsequently, we have to identify the complex roots of the denominator in Eq. (13) with respect to the cavity wavevector, since these represent the lasing condition. If we divide the cavity into a large number of stratified layers, the frequency shift can be numerically calculated with the transfer matrix method by finding the complex roots of t^{-1} or by simply determining the shift of the transmission resonance as the function of the excitation density (neglecting the influence of gain). Both is possible without further approximations, but cannot provide a tuning equation. For deriving an analytic expression, we are interested in a simple form for the final transfer matrix M. Consequently, we will neglect all small contributions of higher order in the following.

Optics EXPRESS

For the determination of the transfer matrix $\mathcal{B}$, we assume that the length of section B is small compared to the THz wavelength $L_B \ll \lambda$ and that the optical excitation is completely absorbed in this section. In Eq. (11), we approximate the cosine by 1 and the sine by its argument. To take into account the change of the dielectric constant by optical excitation, we consider section B as divided into small subsections with a thickness of Δz and then perform the transition to infinitesimal small layer thicknesses dz. The matrix $\mathcal{B}$ is obtained as the product of all sub-matrices, resulting in

$$\mathcal{B} = \prod_{\Delta z \to 0} \begin{pmatrix} 1 & \Delta z \\ -k_B^2 \Delta z & 1 \end{pmatrix} = \begin{pmatrix} 1 & L_B \\ -\int k_B^2(z) dz & 1 \end{pmatrix} . \tag{14}$$

With Eq. (4)

$$\varepsilon(z) = \varepsilon_s \left(1 - \frac{\omega_p^2}{\omega^2}\right) , \tag{15}$$

we can write

$$\mathcal{B} = \begin{pmatrix} 1 & L_B \\ -k_s^2 L_B + k_s^2 \int \frac{\omega_p^2(z)}{\omega^2} dz & 1 \end{pmatrix} \tag{16}$$

with $k_s^2 = \varepsilon_s k_0^2$. Since it will simplify the further derivation significantly without affecting the final result, we first carry out a formal transition $L_B \to 0$

$$\mathcal{B} \overset{L_B \to 0}{=} \begin{pmatrix} 1 & 0 \\ k_s^2 \int \frac{\omega_p^2(z)}{\omega^2} dz & 1 \end{pmatrix} . \tag{17}$$

It might appear inconsistent to set $L_B = 0$ in $\mathcal{B}_{12}$ and $\mathcal{B}_{21}$ but not the integral in $\mathcal{B}_{21}$. The explanation is that the total length L of the cavity must stay the same. Hence, a finite length of section B would have to be compensated by a reduced length of section A. We avoid this compensation, which just complicates the derivation without additional insights, by setting $L_A = L$ in the following. By doing so, we lose terms of higher-order in L_B, which we would otherwise neglect in the final approximation.

To find the transfer matrix for section A, we consider the system to be close to resonance. We write $k_s L = 2\pi N + \delta k_s L$ with N denoting an integer. Since optical gain is required in order to fulfill the lasing condition, δk_s has to be complex. We define $\delta k_s = \Delta k_s - ig/2$ with Δk_s denoting the real component of the wave vector shift and g the threshold gain [31]. Assuming $|\delta k_s L| \ll 1$ we approximate again the cosine by 1 and the sine by its argument resulting in

$$\mathcal{A} = \begin{pmatrix} 1 & \frac{\delta k_s}{k_s} L \\ -\delta k_s k_s L & 1 \end{pmatrix} \tag{18}$$

With Eqs. (17) and (18), the simplified transfer matrix of the total cavity becomes eventually

$$M = \begin{pmatrix} 1 & \frac{\delta k_s}{k_s} L \\ [k_s^2 \int \frac{\omega_p^2}{\omega^2} dz - \delta k_s k_s L] & [1 + \delta k_s k_s L \int \frac{\omega_p^2}{\omega^2} dz] \end{pmatrix} . \tag{19}$$

We now have to determine the complex roots of the denominator in Eq. (13):

$$0 = -M_{21} + k_0^2 M_{12} + i k_0 (M_{11} + M_{22}) . \tag{20}$$

Optics EXPRESS

Inserting the matrix elements and dividing by k_s, we obtain

$$0 = \delta k_s L \left(1 + \frac{k_0^2}{k_s^2}\right) - k_s \int \frac{\omega_p^2}{\omega^2} dz + 2i \frac{k_0}{k_s} + i\delta k_s k_0 L \int \frac{\omega_p^2}{\omega^2} dz \ . \tag{21}$$

In order to fulfill the equation, real and imaginary part on the right side have both to become zero. While the former will yield the frequency shift, the latter will yield an expression for the threshold gain. Since δk_s is complex, both equations are coupled, i.e. there is in principle a gain contribution to the frequency shift and vice versa. However, these contributions are small and we neglect it. Further higher-order coupling terms originate from the imaginary component in the relation $k_s = (n_s - i\frac{g}{2k_0})k_0$ with $n_s = \sqrt{\varepsilon_s}$ which has to be used in the presence of gain. We will neglect the corresponding higher-order coupling terms by the approximation $k_s \approx n_s k_0$. Eventually, we obtain for the real part of Eq. (21)

$$\frac{\Delta k_0}{k_0} = \frac{\Delta \nu}{\nu} \approx \frac{\varepsilon_s}{\varepsilon_s + 1} \frac{1}{L} \int \frac{\omega_p^2}{\omega^2} dz \ . \tag{22}$$

Since $\varepsilon_s \gg 1$ and because we are interested at most in a simple expression describing the behavior qualitatively, we will further approximate the term $\varepsilon_s/(\varepsilon_s + 1)$ by unity. Carrying out the integral by using

$$\omega_p^2 = \frac{n_{eh}(z)e^2}{\varepsilon_0 \varepsilon_s m^*} = \frac{e^2}{\varepsilon_0 \varepsilon_s m^*} \sqrt{\frac{G}{B}} = \frac{e^2}{\varepsilon_0 \varepsilon_s m^*} \sqrt{\frac{\alpha S_0}{B}} \sqrt{e^{-\alpha z}} \ , \tag{23}$$

we eventually obtain

$$\Delta \nu \approx \frac{e^2}{2\pi^2 \varepsilon_0 \varepsilon_s m^*} \frac{1}{L\nu} \sqrt{\frac{S_0}{B\alpha}} \ . \tag{24}$$

Funding

Deutsche Forschungsgemeinschaft (DFG)(HU848/5-1).

Acknowledgment

T. A. acknowledges support by the Helmholtz Research School on Security Technologies. The authors would like to thank W. Anders, M. Höricke, A. Riedel, as well as A. Tahraoui for sample preparation and M. Hempel for fruitful discussions.

References

1. R. Köhler, A. Tredicucci, F. Beltram, H. E. Beere, E. H. Linfield, A. G. Davies, D. A. Ritchie, R. C. Iotti, and F. Rossi, "Terahertz semiconductor-heterostructure laser," Nature **417**, 156–159 (2002).
2. B. S. Williams, "Terahertz quantum-cascade lasers," Nature Photonics **1**, 517–525 (2007).
3. M. S. Vitiello, L. Consolino, S. Bartalini, A. Taschin, A. Tredicucci, M. Inguscio, and P. De Natale, "Quantum-limited frequency fluctuations in a terahertz laser," Nature Photonics **6**, 525–528 (2012).
4. M. Ravaro, S. Barbieri, G. Santarelli, V. Jagtap, C. Manquest, C. Sirtori, S. P. Khanna, and E. H. Linfield, "Measurement of the intrinsic linewidth of terahertz quantum cascade lasers using a near-infrared frequency comb," Opt. Express **20**, 25654–25661 (2012).
5. H.-W. Hübers, S. G. Pavlov, H. Richter, A. D. Semenov, L. Mahler, A. Tredicucci, H. E. Beere, and D. A. Ritchie, "High-resolution gas phase spectroscopy with a distributed feedback terahertz quantum cascade laser," Appl. Phys. Lett. **89**, 061115 (2006).
6. Y. Ren, J. N. Hovenier, R. Higgins, J. R. Gao, T. M. Klapwijk, S. C. Shi, B. Klein, T.-Y. Kao, Q. Hu, and J. L. Reno, "High-resolution heterodyne spectroscopy using a tunable quantum cascade laser around 3.5 THz," Appl. Phys. Lett. **98**, 231109 (2011).
7. L. Consolino, S. Bartalini, H. E. Beere, D. A. Ritchie, M. S. Vitiello, and P. De Natale, "THz QCL-based cryogen-free spectrometer for in situ trace gas sensing", Sensors **13**, 3331–3340 (2013).
8. R. Eichholz, H. Richter, M. Wienold, L. Schrottke, R. Hey, H. T. Grahn, and H.-W. Hübers, "Frequency modulation spectroscopy with a THz quantum-cascade laser", Opt. Express **21**, 32199–32206 (2013).

Optics EXPRESS

9. H. Richter, M. Wienold, L. Schrottke, K. Biermann, H. T. Grahn, and H.-W. Hübers, "4.7-THz local oscillator for the GREAT heterodyne spectrometer on SOFIA," IEEE Trans. Terahertz Sci. Technol. **5**, 539–545 (2015).
10. T. Hagelschuer, M. Wienold, H. Richter, L. Schrottke, K. Biermann, H. T. Grahn, and H.-W. Hübers, "Terahertz gas spectroscopy through self-mixing in a quantum-cascade laser," Appl. Phys. Lett. **109**, 191101 (2016).
11. R. Chhantyal-Pun, A. Valavanis, J. T. Keeley, P. Rubino, I. Kundu, Y. J. Han, P. Dean, L. H. Li, A. G. Davies, and E. H. Linfield, "Gas spectroscopy with integrated frequency monitoring through self-mixing in a terahertz quantum-cascade laser," Opt. Lett. **43**, 2225–2228 (2018).
12. M. Wienold, T. Alam, L. Schrottke, H. T. Grahn, and H.-W. Hübers, "Doppler-free spectroscopy with a terahertz quantum-cascade laser," Opt. Express **26**, 6692–6699 (2018).
13. J. Xu, J. M. Hensley, D. B. Fenner, R. P. Green, L. Mahler, A. Tredicucci, M. G. Allen, F. Beltram, H. E. Beere, and D. A. Ritchie, "Tunable terahertz quantum cascade lasers with an external cavity," Appl. Phys. Lett. **91**, 121104 (2007).
14. A. W. M. Lee, B. S. Williams, S. Kumar, Q. Hu, and J. L. Reno, "Tunable terahertz quantum cascade lasers with external gratings," Opt. Lett. **35**, 910–912 (2010).
15. C. A. Curwen, J. L. Reno, and B. S. Williams, "Terahertz quantum cascade VECSEL with watt-level output power," Appl. Phys. Lett. **113**, 011104 (2018).
16. Q. Qin, B. S. Williams, S. Kumar, J. L. Reno, and Q. Hu, "Tuning a terahertz wire laser," Nature Photonics **3**, 732–737 (2009).
17. N. R. Han, A. de Geofroy, D. P. Burghoff, C. W. I. Chan, A. W. M. Lee, J. L. Reno, and Q. Hu, "Broadband all-electronically tunable MEMS terahertz quantum cascade lasers," Opt. Lett. **39**, 3480–3483 (2014).
18. K. Ohtani, M. Beck, and J. Faist, "Electrical laser frequency tuning by three terminal terahertz quantum cascade lasers," Appl. Phys. Lett. **104**, 011107 (2014).
19. I. Kundu, P. Dean, A. Valavanis, L. Chen, L. H. Li, J. E. Cunningham, E. H. Linfield, and A. G. Davies, "Discrete Vernier tuning in terahertz quantum cascade lasers using coupled cavities," Opt. Express **22**, 16595–16605 (2014).
20. D. Turčinková, M. I. Amanti, G. Scalari, M. Beck, and J. Faist, "Electrically tunable terahertz quantum cascade lasers based on a two-sections interdigitated distributed feedback cavity," Appl. Phys. Lett. **106**, 131107 (2015).
21. I. Kundu, P. Dean, A. Valavanis, J. R. Freeman, M. C. Rosamond, L. H. Li, Y. J. Han, E. H. Linfield, and A. G. Davies, "Continuous frequency tuning with near constant output power in coupled y-branched terahertz quantum cascade lasers with photonic lattice," ACS Photonics **5**, 2912–2920 (2018).
22. D. Turčinková, M. I. Amanti, F. Castellano, M. Beck, and J. Faist, "Continuous tuning of terahertz distributed feedback quantum cascade laser by gas condensation and dielectric deposition," Appl. Phys. Lett. **102**, 181113 (2013).
23. L. A. Dunbar, R. Houdré, G. Scalari, L. Sirigu, M. Giovannini, and J. Faist, "Small optical volume terahertz emitting microdisk quantum cascade lasers," Appl. Phys. Lett. **90**, 141114 (2007).
24. C. Zervos, M. D. Frogley, C. C. Phillips, D. O. Kundys, L. R. Wilson, M. Hopkinson, and M. S. Skolnick, "All-optical switching in quantum cascade lasers," Appl. Phys. Lett. **90**, 053505 (2007).
25. G. Chen, R. Martini, S.-w. Park, C. G. Bethea, I.-C. A. Chen, P. D. Grant, R. Dudek, and H. C. Liu, "Optically induced fast wavelength mAppl. Phys. Lett." **97**, 011102 (2010).
26. S. Suchalkin, S. Jung, R. Tober, M. A. Belkin, and G. Belenky, "Optically tunable long wavelength infrared quantum cascade laser operated at room temperature," Applied Physics Letters **102**, 011125 (2013).
27. D. K. Guo, H. Cai, M. A. Talukder, X. Chen, A. M. Johnson, J. B. Khurgin, and F.-S. Choa, "Near-infrared induced optical quenching effects on mid-infrared quantum cascade lasers," Appl. Phys. Lett. **104**, 251102 (2014).
28. M. Hempel, B. Röben, L. Schrottke, H.-W. Hübers, and H. T. Grahn, "Fast continuous tuning of terahertz quantum-cascade lasers by rear-facet illumination," Appl. Phys. Lett. **108**, 191106 (2016).
29. M. Hempel, B. Röben, M. Niehle, L. Schrottke, A. Trampert, and H. T. Grahn, "Continuous tuning of two-section, single-mode terahertz quantum-cascade lasers by fiber-coupled, near-infrared illumination," AIP Advances **7**, 055201 (2017).
30. H. M. Pickett, R. L. Poynter, E. A. Cohen, M. L. Delitsky, J. C. Pearson, and H. S. P. Müller, "Submillimeter, millimeter, and microwave spectral line catalog," J. Quant. Spectrosc. Radiat. Transfer **60**, 883–890 (1998).
31. S. L. Chuang, *Physics of photonic devices* (Wiley, 2009), 2nd ed.
32. C. H. Henry and D. Lang, "Nonradiative capture and recombination by multiphonon emission in GaAs and GaP," Phys. Rev. B **15**, 989–1016 (1977).
33. Y. P. Varshni, "Band-to-band radiative recombination in groups IV, VI, and III-V semiconductors (i)," physica status solidi (b) **19**, 459–514 (1967).
34. M. Born and E. Wolf, *Principles of Optics* (Cambridge University, 1999), 7th ed.
35. M. Levinshtein, S. Rumyantsev, and M. Shur, eds., *Handbook series on semiconductor parameters*, vol. 1 (World Scientific, 1996).
36. S. Barbieri, J. Alton, H. E. Beere, J. Fowler, E. H. Linfield, and D. A. Ritchie, "2.9 THz quantum cascade lasers operating up to 70 K in continuous wave," Appl. Phys. Lett. **85**, 1674–1676 (2004).
37. M. Wienold, L. Schrottke, M. Giehler, R. Hey, W. Anders, and H. T. Grahn, "Low-voltage terahertz quantum-cascade lasers based on LO-phonon-assisted interminiband transitions," Electron. Lett. **45**, 1030–1031 (2009).
38. M. Rösch, G. Scalari, M. Beck, and J. Faist, "Octave-spanning semiconductor laser," eNature Photonics **9**, 42–47 (2015).